ON THE COMPUTATION OF THE VELOCITY FIELDS AND THE DYNAMIC FREE SURFACE GENERATED IN A LIQUID METAL COLUMN BY A ROTATING MAGNETIC FIELD

N. Saluja, O.J. Ilegbusi, and J. Szekely

Department of Materials Science and Engineering • Massachusetts Institute of Technology • 77 Massachusetts Avenue • Cambridge • MA 02139, USA.

ON THE COMPUTATION OF THE VELOCITY FIELDS AND THE DYNAMIC FREE SURFACE GENERATED IN A LIQUID METAL COLUMN BY A ROTATING MAGNETIC FIELD

ABSTRACT

A mathematical formulation is given and computed results are presented describing the electromagnetic force field and the velocity field in a cylindrical metal column which is being stirred by a rotating magnetic field. The particular features of this work are that an allowance has been made for both free surface deformation and the coupling between the magnetic field and the velocity field. The computed results are in apparent agreement with the earlier work of Davidson and Hunt regarding the existence of secondary flows in these systems. It is shown, however, that significant free surface deformation may occur in many cases, which will affect the velocity field particularly in the vicinity of the free surface. Indeed, serious errors may be introduced in the calculation of the velocity fields if a flat free surface is artificially imposed as part of the computational scheme.

1. Introduction

The velocity fields produced in a liquid metal column by a rotating electromagnetic field have attracted a great deal of attention because of the major practical application of these phenomena in the electromagnetic stirring of liquid metal pools in continuous casting molds (see Poole 1986 ; Tzavaras & Brody 1984). Much of the work to - date has been computational (Ilegbusi & Szekely 1989 ; Spitzer, Dubke & Schwerdtfeger 1986), with a limited number of experimental measurements (Robinson 1973), and elegant order of magnitude approximations (Moffat 1965 ; Sneyd 1971). As a result of this work, there exists a reasonably good, semi - quantitative understanding of the flow phenomena in these systems. However, two potentially important aspects of this problem remained relatively unexplored up to the present time. One of these is related to the secondary flows that may be produced by axial variations in the rotating field, these being necessarily associated with the discontinuities at the free surface of the melt; the other is associated with the free surface disturbances.

In a recent paper, Davidson & Hunt (1987) developed analytical concepts to represent the velocity fields and to define the key regions of behavior in molten metal columns agitated by a rotating magnetic field. The principal findings of their work may be summarized as follows:

- The discontinuities in the magnetic field at the free surface of the metal and at the edge of the stirrer may give rise to secondary flows. This is an important, hitherto not available finding.
- By the elegant manipulation of the governing equations and by making order of magnitude estimates the authors were able to make fairly good predictions for both the velocities and the magnetic force field components.
- The authors also used the k-ε model (see Launder & Spalding 1972) and the FLUENT computational package to compute the velocity fields and obtained not unreasonable agreement between measurements and predictions.

This elegant work has provided useful insights, but should be capable of extension in the following areas, which is the purpose of the present paper:

- The linear approximation for the radial dependence of the azimuthal electromagnetic force was a significant oversimplification, clearly stated by Davidson & Hunt (1987). The retention of the subsequent terms of the series, as will be done here, will relax this assumption (see Saluja, Ilegbusi & Szekely 1990).

- In the formulation developed by Davidson & Hunt (1987), the coupling between the velocity and the magnetic fields has been neglected. As recently shown by the present authors, this assumption need not be accurate (Saluja et al. 1990, Saluja 1991).
- Both the calculations and the experiments performed by the authors involved a rigid free surface. This is clearly not the case in most practical applications of electromagnetic stirring; indeed, free surface disturbances are thought to constitute one of the major practical problems in mold stirring devices. In the formulation to be developed here, proper allowance will be made for free surface effects. The force field discontinuities mentioned earlier may have their most profound effect in generating free surface disturbances.
- In a general sense, it is always desirable to complement analytical asymptotic solutions with those computed, with fewer restrictive simplifying assumptions; analysis and machine computation should be regarded as complementary techniques in tackling most fluid flow problems.

2. Formulation

2.1 Order of Magnitude Analysis

Figure 1 shows the schematic of a system in which a rotating magnetic field is applied to a melt contained in a mold. Electromagnetic stirring of the melt produces a dominant velocity in the azimuthal direction, and causes the free surface to deform as shown.

Ignoring axial gradients of the forces, we can consider the pressure difference that arises from the centrifugal force:

$$\Delta p = \frac{1}{2}\rho u^2$$

If the characteristic velocity u ~ 100 cm/s, and fluid density ρ ~ 7.022 g/cm^3, we get the pressure difference Δp ~ 3.5×10^4 dynes/cm^2. The height of the free surface, h, that can be supported by this pressure difference is then given by the hydrostatic balance equation:

$$\Delta p = \rho g h$$

For an idealized situation where axial gradients of the forces are absent, this yields a value of h ~ 5 cm. Such an analysis may have limited practical applicability, but nevertheless provides a good first approximation.

To compare the relative effects of surface tension, we can evaluate a typical effective pressure difference:

$$\Delta p = \frac{\sigma_t}{r_o}$$

where σ_t is the surface tension coefficient of molten steel and r_o is the inner radius of the mold. This yields a value of Δp ~ 400 dynes/cm^2. Thus, for the above parameters, surface tension forces are quite negligible. However, for low melt velocities (corresponding to low magnetic field strength and/or low frequency of applied current), ignoring these effects will introduce substantial error in the computation. The neglect of wall adhesion effects can also introduce errors in the immediate vicinity of the walls.

The computed results have been compared to existing analytical expressions for melt velocity available in literature. In particular, Davidson (1985) gives an expression for the maximum velocity as:

$$v_{max} = \overline{V}\Omega_s \cosh\left(\sqrt{2}\right)$$

where $\overline{V}$ is a characteristic velocity given by:

$$\overline{V} = B_o r_o \sqrt{\frac{\sigma\omega}{\rho}}$$

in which B_o is the applied magnetic field, σ is the electrical conductivity, and ω is the angular velocity of the applied current. Ω_s can be obtained from the following expression:

$$\Omega_s^2 = \frac{1}{2}\int_0^{\infty} \phi\left(\frac{\Delta z}{r_o}\right) d\left(\frac{\Delta z}{r_o}\right)$$

where $\phi(\Delta z/r_o)$ is the axial variation of forces as a function of Δz, the vertical distance between the edge of the stirrer and the point at which forces are being computed (see §2C). For a steel

melt with B_o = 0.05 tesla, r_o = 0.2 m, applied current frequency f = 20 Hz, and a fourth power-law axial decay function of forces, the maximum bulk velocity is ~ 2.5 m/s. As will be shown later, this value falls well within the range of results obtained from numerical calculations.

While these calculations have been very helpful, it is an inherent aspect of work of this kind that many potentially important aspects of the process had to be neglected in order to obtain these simple predictive expressions.

Previous investigators (Davidson 1985 ; Davidson & Boysan 1987 ; Davidson 1988) have used arguments based on dimensional analysis to give order of magnitude estimates and comparison for velocities in the system. However, many aspects of the process have been completely neglected. The free surface behavior in electromagnetic stirring applications is also complicated due to the following reasons:

- The surface tension effects become significant, specially at low magnetic fields and at low frequencies of the applied current.
- Contact angle effects are important at near-wall regions, and these may significantly affect the free surface shape, specially at low melt velocities.
- Small-scale oscillations at the free surface are present even when the melt velocities in the main body of the system have reached a steady state, and these cannot be predicted by classical or analytical solutions.
- The axial gradients in the electromagnetic forces due to edge-effects at the vicinity of the free surface also modify the velocity fields and free surface deformation in the system.

In many practical applications of stirring including continuous casting, the applied magnetic field extends over a finite domain and there are regions where the induced electromagnetic forces are practically zero. This axial variation of swirl drives secondary flows which superimpose on the primary azimuthal flow to create a complex fluid flow pattern.

It has been shown that the axial variation of forces creates a recirculating flow pattern in a plane perpendicular to the azimuthal direction (Davidson & Hunt 1987 ; Davidson & Boysan 1987). However, free surface effects on this recirculating flow have not been the focus of attention until now. Indeed, the free surface deformation can markedly alter the nature of these secondary flows.

2.2 Fluid Flow Equations

A general formulation of the governing fluid flow equations is presented in this section. Specifically, the incorporation of terms representing fractional areas and fractional volume open to fluid flow in these equations give the formulation more universality. The equation governing the fractional volume of fluid is used for tracking the free surface.

The equations for fluid flow can be represented by the mass continuity equation, the equations of motion for the cylindrical geometry, the equation for fluid fraction, and the equations representing the k-ε turbulence model.

Equation of mass continuity:

$$\frac{\partial}{\partial r}(uA_r)+\frac{1}{r}\frac{\partial}{\partial \theta}(vA_\theta)+\frac{\partial}{\partial z}(wA_z)+\frac{uA_r}{r}=0 \tag{1}$$

where u,v,w are the velocities, and A_r, A_θ, A_z are the fractional areas open to flow in the coordinate directions r,θ,and z respectively.

Equation of motion in the radial direction:

$$\frac{\partial u}{\partial t}+\frac{1}{V}\left\{uA_r\frac{\partial u}{\partial r}+\frac{vA_\theta}{r}\frac{\partial u}{\partial \theta}+wA_z\frac{\partial u}{\partial z}\right\}-\frac{A_\theta v^2}{rV}=-\frac{1}{\rho}\frac{\partial p}{\partial r}+G_r+f_r \tag{2}$$

Equation of motion in the azimuthal direction:

$$\frac{\partial v}{\partial t}+\frac{1}{V}\left\{uA_r\frac{\partial v}{\partial r}+\frac{vA_\theta}{r}\frac{\partial v}{\partial \theta}+wA_z\frac{\partial v}{\partial z}\right\}+\frac{A_\theta uv}{rV}=-\frac{1}{\rho r}\frac{\partial p}{\partial \theta}+G_\theta+f_\theta \tag{3}$$

Equation of motion in the axial direction:

$$\frac{\partial w}{\partial t}+\frac{1}{V}\left\{uA_r\frac{\partial w}{\partial r}+\frac{vA_\theta}{r}\frac{\partial w}{\partial \theta}+wA_z\frac{\partial w}{\partial z}\right\}=-\frac{1}{\rho}\frac{\partial p}{\partial z}+G_z+f_z \tag{4}$$

where V is the fractional volume open to flow, t is the time, and p is the static pressure. G_r, G_θ, G_z are the body accelerations and f_r, f_θ, f_z are the viscous accelerations. G_r and G_θ are due

to electromagnetic forces, whereas G_z is due to gravity forces. The viscous accelerations for a variable dynamic viscosity μ, are given by the following equations:

$$\rho V f_r = -\left\{\frac{\partial}{\partial r}(A_r\tau_{rr}) + \frac{1}{r}\frac{\partial}{\partial\theta}(A_\theta\tau_{r\theta}) + \frac{\partial}{\partial z}(A_z\tau_{rz}) + \frac{1}{r}(A_r\tau_{rr} - A_\theta\tau_{\theta\theta})\right\} \tag{5}$$

$$\rho V f_\theta = -\left\{\frac{\partial}{\partial r}(A_r\tau_{r\theta}) + \frac{1}{r}\frac{\partial}{\partial\theta}(A_\theta\tau_{r\theta}) + \frac{\partial}{\partial z}(A_z\tau_{rz}) + \frac{1}{r}(A_r + A_\theta)\tau_{r\theta}\right\} \tag{6}$$

$$\rho V f_z = -\left\{\frac{\partial}{\partial r}(A_r\tau_{rz}) + \frac{1}{r}\frac{\partial}{\partial\theta}(A_\theta\tau_{\theta z}) + \frac{\partial}{\partial z}(A_z\tau_{zz}) + \frac{A_r\tau_{rz}}{r}\right\} \tag{7}$$

The stress terms in Equations (5), (6), and (7) are given by the following:

Normal Stresses:

$$\tau_{ii} = -2\mu\left[R_i\frac{\partial u_i}{\partial x_i} + \xi_{ij}\frac{u_j}{x_j}\right] \tag{8}$$

Shear stresses:

$$\tau_{ij} = -\mu\left[\frac{\partial u_j}{\partial x_i} + R_j\frac{\partial u_i}{\partial x_j} + \xi_{ij}\frac{u_j}{x_i}\right] \tag{9}$$

where

$$i, j \equiv r, \theta, z; R_r = R_z = 1; R_\theta = \frac{1}{r}; \xi_{rz} = \xi_{\theta z} = 0; \xi_{r\theta} = 1.$$

The volume of fluid function, $F(r,\theta,z,t)$, represents the volume of fluid per unit volume and satisfies the equation:

$$\frac{\partial F}{\partial t} + \frac{1}{V}\left[\frac{\partial}{\partial r}(FA_r u) + \frac{1}{r}\frac{\partial}{\partial\theta}(FA_\theta v) + \frac{\partial}{\partial z}(FA_z w) + \frac{FA_r u}{r}\right] = 0 \tag{10}$$

where

$$F\begin{cases} = 1 & \text{cell full of fluid} \\ 0 < F < 1 & \text{free surface exists} \\ = 0 & \text{void region} \end{cases}$$

'Voids' represent regions without any fluid mass that have a uniform pressure assigned to them. Physically, they represent regions filled with a vapor or gas whose density is insignificant compared to the fluid density.

The Reynolds stresses are estimated using the standard k-ε model. The coefficient of dynamic viscosity is assumed to be a sum of the molecular and turbulent viscosities:

$$\mu = \rho(\nu_T + \nu_M) \tag{11}$$

where ν_T and ν_M are the turbulent and molecular kinematic viscosities respectively.

The turbulence viscosity can be expressed as a function of k, the turbulence kinetic energy, and ε, the turbulence energy dissipation function, as follows:

$$\nu_T = C_\nu \frac{k^2}{\varepsilon} \tag{12}$$

where C_ν is an empirical constant.

The turbulence kinetic energy per unit mass is governed by the equation:

$$\frac{\partial k}{\partial t} + \frac{1}{V}\left[uA_r \frac{\partial k}{\partial r} + \frac{vA_\theta}{r}\frac{\partial k}{\partial \theta} + wA_z \frac{\partial k}{\partial z}\right] = P + D_k - \varepsilon \tag{13}$$

where P is the shear production term and D_k is the diffusion term. These terms are defined by the following equations:

$$\begin{aligned} P = C_K\left(\frac{\mu}{\rho V}\right)\Bigg[& 2A_r\left(\frac{\partial u}{\partial r}\right)^2 + 2A_\theta\left(\frac{1}{r}\frac{\partial v}{\partial \theta} + \frac{u}{r}\right)^2 + 2A_z\left(\frac{\partial w}{\partial z}\right)^2 \\ & + \left(\frac{\partial v}{\partial r} + \frac{1}{r}\frac{\partial u}{\partial \theta} - \frac{v}{r}\right)\left\{A_r\frac{\partial v}{\partial r} + A_\theta\left(\frac{1}{r}\frac{\partial u}{\partial \theta} - \frac{v}{r}\right)\right\} \\ & + \left(\frac{\partial u}{\partial z} + \frac{\partial w}{\partial r}\right)\left(A_z\frac{\partial u}{\partial z} + A_r\frac{\partial w}{\partial r}\right) \\ & + \left(\frac{\partial v}{\partial z} + \frac{1}{r}\frac{\partial w}{\partial \theta}\right)\left(A_z\frac{\partial v}{\partial z} + \frac{A_\theta}{r}\frac{\partial w}{\partial \theta}\right)\Bigg] \end{aligned} \tag{14}$$

$$D_k = \frac{1}{V}\left[\frac{\partial}{\partial r}\left(\nu_q A_r \frac{\partial k}{\partial r}\right) + \frac{1}{r}\frac{\partial}{\partial \theta}\left(\frac{\nu_q A_\theta}{r}\frac{\partial k}{\partial \theta}\right) + \frac{\partial}{\partial z}\left(\nu_q A_z \frac{\partial k}{\partial z}\right) + \frac{\nu_q A_r k}{r}\right] \tag{15}$$

C_k is an empirical constant. In the above equation, ν_q is a diffusion coefficient which is defined as:

$$\nu_q = C_{mk}\left(\frac{\mu}{\rho}\right) \tag{16}$$

where C_{mk} is an empirical constant.

The transport equation for turbulence dissipation can be expressed as:

$$\frac{\partial \varepsilon}{\partial t} + \frac{1}{V}\left[uA_r \frac{\partial \varepsilon}{\partial r} + \frac{vA_\theta}{r}\frac{\partial \varepsilon}{\partial \theta} + wA_z \frac{\partial \varepsilon}{\partial z}\right] = \frac{C_{\varepsilon 1}\varepsilon P}{k} + D_\varepsilon - \frac{C_{\varepsilon 2}\varepsilon^2}{k} \tag{17}$$

where $C_{\varepsilon 1}$ is the coefficient of production, and $C_{\varepsilon 2}$, is the coefficient of decay. The production term P is similar to that given by Equation (14), and the diffusion term D_ε is similar to the expression of Equation (15), with k replaced by ε and with the constant C_{mk} replaced with another constant $C_{m\varepsilon}$. The values of the turbulence constants used are given in Table 1.

2.3 Electromagnetic Forces

The electromagnetic force field may be calculated with the aid of Maxwell's equations and the Ohm's Law. Upon applying the magnetoquasistatic approximation, we have the following:

Equation of magnetic flux continuity:

$$\vec{\nabla} \cdot \vec{B} = 0 \tag{18}$$

Ampere's Law:

$$\vec{J} = \vec{\nabla} \times \vec{H} \tag{19}$$

Faraday's Law:

$$\vec{\nabla} \times \vec{E} = -\frac{\partial \vec{B}}{\partial t} \tag{20}$$

Ohm's Law:

$$\vec{J} = \sigma\left[\vec{E} + \left(\vec{u} \times \vec{B}\right)\right] \tag{21}$$

where $\vec{E}$ is the electric field, $\vec{H}$ is the magnetic field strength, $\vec{B}$ is the magnetic flux density, $\vec{J}$ is the induced current density, and $\vec{u}$ is the velocity vector.

The electromagnetic body force $\vec{F}$ may be calculated from the following relationship:

$$\vec{F} = \vec{J} \times \vec{B} \tag{22}$$

When a rotating magnetic field is applied to an infinitely long cylindrical system, the induced current density has an axial component, whereas the induced magnetic flux density has both radial and azimuthal components. In addition, the dominant velocity is in the azimuthal direction, and all derivatives with respect to the axial coordinate are zero. We get the following partial differential equation for the radial component of the magnetic induction, B_r (Saluja, Ilegbusi & Szekely 1990):

$$\frac{1}{\mu_o r}\left[\frac{\partial}{\partial r}\left\{r\frac{\partial}{\partial r}(rB_r)\right\} + \frac{\partial B_r}{\partial \theta}\right] = \sigma\left[r\frac{\partial B_r}{\partial t} + v\frac{\partial B_r}{\partial \theta}\right] \tag{23}$$

If a sinusoidal variation of the magnetic induction with time and the azimuthal coordinate is assumed, the following similarity transformation can be applied to the above equation (see Spitzer et al. 1986):

$$\eta = \frac{irB_r}{p} e^{-i(\omega t - p\theta)} \tag{24}$$

The boundary condition applicable in the above case is:

$$B_r(r = r_o) = B_o \cos(\omega t - p\theta) \tag{25}$$

where B_o is the applied amplitude of B_r, p is the number of pole pairs, and $i = \sqrt{-1}$.

Using the similarity transformation, Equation (23) can be expressed as:

$$\eta'' + \frac{\eta'}{r} - \left[i\gamma^2 + \frac{p^2}{r^2} \right] \eta = 0 \tag{26}$$

where $p = \pm\kappa$, with $\omega^* = (\omega - pv/r)$ and $\gamma = (\sigma\mu_o\omega^*)^{1/2}$. The above equation has to be solved with the following boundary conditions:

$$\eta(r = r_o) = \frac{iB_o r_o}{p} \tag{27}$$

$$\eta(r = 0) = 0 \tag{28}$$

It should be noted that in Equation (26), γ is a function of the azimuthal velocity, which varies both spatially and with time. This necessitates the coupling of this equation with the velocity field. In an explicit algorithm, this requires updating the forces in accordance with the velocities at every iteration of each time step.

Using Bessel functions with the appropriate boundary conditions yields a solution of the form:

$$\eta = \frac{iB_o r_o J_p\left(r\gamma i^{\frac{3}{2}} \right)}{pJ_p\left(r_o \gamma i^{\frac{3}{2}} \right)} \tag{29}$$

which can be rewritten as

$$\eta = \varsigma \frac{J_p\left\{ \mathrm{Re}_m^{0.5} \left(\frac{r}{r_o} \right) i^{\frac{3}{2}} \right\}}{J_p\left\{ \mathrm{Re}_m^{0.5} i^{\frac{3}{2}} \right\}} \tag{30}$$

where $Re_m = \omega^* \sigma\mu_o r_o^2$, is an 'effective' magnetic Reynolds number, and $\varsigma = iB_o r_o/p$.

The infinite series in the numerator and denominator of Equation (30) can be split up into the real and imaginary parts, called Φ_{Re} and Φ_{Im} respectively.

$$J_p\left(i^{\frac{3}{2}}\Theta\right)=i^{\frac{3p}{2}}\left[\Phi_{\mathrm{Re}}+\Phi_{\mathrm{Im}}\right] \tag{31}$$

where

$$\Phi_{\mathrm{Re}}=\sum_{k=0}^{\infty}\frac{(-1)^k\Theta^{p+4k}}{2^{p+4k}\Gamma(2k+1)\Gamma(p+2k+1)} \tag{32}$$

$$\Phi_{\mathrm{Im}}=i\sum_{k=0}^{\infty}\frac{(-1)^k\Theta^{p+2+4k}}{2^{p+2+4k}\Gamma(2k+2)\Gamma(p+2k+2)} \tag{33}$$

To find , η' that is, the derivative of η with respect to the radial coordinate, Equation (30) can be differentiated. It should be noted that the denominator in the expression for η is independent of r, and the chain rule of differentiation gives:

$$\frac{d}{dr}\left[J_p\left(i^{\frac{3}{2}}\Theta\right)\right]=\frac{d}{d\Theta}\left[J_p\left(i^{\frac{3}{2}}\Theta\right)\right]\times\frac{d\Theta}{dr} \tag{34}$$

The expressions for the electromagnetic body forces as defined by Equation (22) are thus:

$$F_r=-\sigma\omega^{\bullet}\left[\left(\frac{NQ-MP}{2}\right)\sin 2\delta-NP\cos^2\delta+MQ\sin^2\delta\right] \tag{35}$$

$$F_\theta=\frac{p\sigma\omega^{\bullet}}{r}(N\cos\delta+M\sin\delta)^2 \tag{36}$$

where $\eta=M+iN;\ \eta'=P+iQ;\ \delta=\omega t-p\theta$

The assumption of an infinitely long cylindrical system allows simplification of the Maxwell's equations. However, the stirrer has a finite size, and the associated edge-effects give rise to axial gradients in the forces which have to be accounted for. The quantities G_r and G_θ in Equations (2) and (3) respectively can be expressed as:

$$G_{r,\theta}=\frac{F_{r,\theta}}{\rho}\times\phi\left(\frac{\Delta z}{r_o}\right) \tag{37}$$

$\phi(\Delta z/r_O)$ represents the axial variation of the forces as a function of Δz, the vertical distance between the edge of the stirrer and the point at which forces are being computed. According to

a suggestion by Davidson & Hunt (1987) this variation is expressed as a fourth power-law decay:

$$\phi\left(\frac{\Delta z}{r_o}\right)=\begin{cases}\left(1+\left(\frac{z_{top}-z}{r_o}\right)^4\right)^{-1} & z > z_{top} \\ 1.0 & z_{bot} \le z \le z_{top} \\ \left(1+\left(\frac{z-z_{bot}}{r_o}\right)^4\right)^{-1} & z < z_{bot}\end{cases} \qquad (38)$$

where z_{top} and z_{bot} respectively denote the height of the top and bottom geometrical edges of the stirrer. In this paper, we shall use one pair of poles for the calculation of the electromagnetic force field.

This formulation to represent electromagnetic forces relaxes assumptions made by previous investigators, namely the linear dependence of the azimuthal force density on the radial distance, and the decoupling of the electromagnetic and velocity fields. Significant error may be introduced by these simplifications, as has been shown by Saluja et al. (1990).

2.4 Boundary Conditions

The boundary conditions are the following:

- symmetry about the centerline: no normal fluxes

- no slip at the solid boundaries introduced through the wall functions
  It is assumed that (a) the velocity profile obeys the logarithmic law, (b) the turbulence energy is proportional to the wall shear stress, and, (c) the length scale is proportional to the distance from the wall.

These assumptions lead to the following expressions:

$$\frac{u}{\sqrt{\frac{\tau}{\rho}}}=\frac{1}{\mathrm{K}}\ln\left[E\left(\frac{y\sqrt{\tau\rho}}{\mu}\right)\right] \qquad (39)$$

from which the wall shear stress τ can be determined from the velocity u. In Equation (39), K is the von Karman constant (= 0.41) and E is the roughness parameter (= 9.8 for smooth walls.) Both K and E are empirically obtained dimensionless numbers.

$$k = C_v^{-1/2} \frac{\tau}{\rho} \tag{40}$$

which enables the energy k to be deduced from τ, and,

$$\varepsilon = \frac{C_v^{3/4} k^{3/2}}{K y_p} \tag{41}$$

which serves as the third boundary condition. In Equation (41), y_p is the distance from the wall.

- free surface
  The tangential stresses at the free surface are set to zero (Nichols, Hirt & Hotchkiss 1980). Surface tension is incorporated using an equivalent surface pressure $p_s = -\sigma_t K_c$, where K_c is the local curvature in each boundary cell. This is done for all interface cells except near the walls where the wall adhesion effects have to be represented. The pressure p_s is then simply used as an applied surface pressure. In addition, if the pressure of the void cells next to the interface is specified, it is also included in the surface pressure term.

3. Method of Solution

The input parameters used in the computations are summarized in Table 2.

The equations are solved using FLOW-3D, a program which has enhanced free surface capabilities. The interface tracking is done using VOF (volume of fluid) method of Hirt and Nichols (1981). It should be noted that volume tracking methods like the one used cannot resolve details of the interface that are smaller than the mesh size (see Floryan and Rasmussen 1989).

The domain of calculation includes the fluid body and the gas in the mold above the fluid. These extra cells in the computational mesh, which are initially occupied by the ambient, are used to accommodate the free surface deformation.

Electromagnetic forces are a function of the electrical conductivity of the fluid. Hence the forces acting on fluid cells are proportional to the volume of fluid contained in them. The stirring speed is approximately proportional to $\sigma^{1/2}$ (Kitagawa et al. 1983), other electrical parameters being constant. The electrical conductivity of the void regions is extremely low, and hence the electromagnetic forces in the void regions drop to negligibly low values. This gives rise to steep gradients in forces at the melt/ambient interface. This might lead to some computational instabilities, and requires the use of free surface algorithms which are more robust and can handle large free surface deformations.

Two sets of calculations are performed. In the first, a $10 \times 10 \times 20$ grid was used, the larger number of grids being used in the axial direction. The imposed time step size was ~ 100 μs, and the simulation required 80 hours of CPU time on the VAXstation 3100 workstation. This corresponds to a real time of four seconds. In the second set of computations, a 20×30 axi-symmetric grid was used. Because of stability considerations, the imposed time step size was ~ 10 μs. This made the calculations very time-intensive; 130 hours of CPU time on a VAXstation 3100 Model 38 were required to simulate the process behavior for a real time of two seconds.

4. Computed Results

In the following we shall present a selection of the computed results and these will seek to address two specific aspects of the problem, namely :

- the behavior of the free surface in rotary stirring
- the calculation of both the azimuthal and the axial velocities in the vicinity of the free surface.

This is an important, hitherto little explored problem, which has considerable practical and fundamental interest. The practical interest is provided by two factors. One of these is that in most practical applications of electromagnetic stirring in continuous casting, free surface deformation and free surface disturbances are generally thought to be undesirable because of the possible contamination of the metals to be processed. Indeed, the avoidance of these free surface disturbances tends to pose a practical limitation on the stirring rates that may be achieved. The second point is that if a simple rotating motion were to exist at the free surface, a parabolic shape would be generated, the geometry of which should provide a convenient estimate of the rate of rotation.

In virtually all the work done to date a flat free surface has been postulated; in their recent paper Davidson & Hunt (1987) described a laboratory scale system, where such conditions were indeed imposed. This provided the ideal data for testing a model, but perhaps at the expense of providing a faithful representation of rotating motion in real electromagnetically stirred systems of industrial interest.

In the results that follow, normalized coordinates have been used in the axial and radial directions. Thus, $z^* = z/h_m$, and $r^* = r/r_o$, where h_m is the height of the mold.

Table 3 (Case 1) gives the geometry used in the first set of calculations. The attenuation effects of the 1 cm thick copper mold have been taken into account by the use of an effective magnetic field, which is calculated from the boundary conditions for the magnetic field intensity and it's derivatives at the mold/metal interface. Neglecting the field losses in the copper mold would significantly overestimate the melt velocities and the free surface deformation.

Figure 2 shows the computed velocity fields in the system up to about 4 seconds of real time, which corresponds to the attainment of a "quasi - steady" state.

A more detailed description of the free surface is shown in Figure 3, where the velocity fields in the vicinity of the free surface are more readily observable.

Inspection of these figures is instructive, because it shows that quite large free surface deformation occurs for the conditions examined; furthermore, a finite time is required for the attainment of these free surface conditions. It is also seen that quite significant vertical velocity components exist in the system. As discussed in an earlier paper by Davidson & Hunt (1987), and also by the present authors, these are attributable to the "end effects."

Figure 4 shows the calculated velocity fields when the free surface is replaced by a flat free-shear surface. This is the boundary condition which has been used by virtually all previous investigators. It is seen that the velocity fields obtained are markedly different from Figure 3, and proves that unless allowance for free surface deformation is made, it will lead to falsification of the velocity field in the vicinity of the top surface.

It is this seen that the neglect of free surface deformation could introduce serious errors not only regarding the actual position of the free surface, but also regarding the nature of the

velocity field in the vicinity of the free surface. Indeed, as reported by Sahajwala et al. (1989) for a gas plume stirred system, the artificial imposition of a flat free surface,. e.g. for the sake of mathematical convenience, when such a situation does not exist, may seriously distort the whole flow field.

While the vector plots given are helpful in identifying the melt velocities it may be useful to show these quantities explicitly. Figure 5 shows the history plot of the azimuthal velocity at a monitored location. Figure 6 shows azimuthal velocity profile in the radial direction at a fixed time of 4 seconds.

Figure 7 shows the axial velocity profile in the radial direction at a time equal to 3 seconds. The axial velocity is monitored at a height of 15 cm from the bottom inner surface of the mold, and this corresponds to a location in the 'forced region', that is, within the axial geometrical limits of the stirrer. It is seen that even in the forced region, significant axial velocities exist. However, the magnitude of the axial velocities is smaller than the azimuthal velocities in the system, which is contrary to what has been reported by Davidson (1988).

Figures 8 and 9 show the radial profiles of the turbulence kinetic energy and the turbulence energy dissipation respectively.

Previous results show that significant free surface deformation occurs even at moderate velocities. It is thus instructive to explore a situation where the velocities are much higher, leading to more severe free surface deformation. The altered geometry of the system (see Case 2 in Table 3) also results in more pronounced secondary flows.

Figure 10 shows the computed velocity fields at 0.5 seconds. For sake of clarity, the regions next to the free surface and below the stirrer are magnified to give a better idea of the velocity vectors and their relative magnitudes. The maximum axial velocity in the system is ~ 0.25 m/s whereas the maximum azimuthal velocity is ~ 1.5 m/s.

Figure 11 shows the velocity fields at a time of 1.0 seconds. The secondary flows in the system are now more pronounced, and the free surface has further deformed to achieve a 'crater' like shape characteristic of a rotating fluid.

Figure 12 shows the velocity vectors at a time of 2.0 seconds. The free surface is seen to be severely deformed. The flow pattern near the free surface is seen to be quite complex. The fluid near the bottom of the mold has relatively low axial velocities.

Figure 13 shows the axial variation of the forces. It is seen that the forces drop to almost zero at a distance of ~ $2r_o$ from the bottom and top of the stirrer. It should be noted that the exact nature of this function should be determined experimentally, because the rate of decay of the forces with axial distance can significantly alter the velocities in the system.

Figure 14 shows the evolution of the azimuthal velocity in the system for a location near the mold wall at two different heights. The azimuthal velocities in the forced region are higher than in the location below the stirrer, while the opposite is true for axial velocities, as seen from Figure 15.

The radial profile of the azimuthal velocity at two different times is shown in Figure 16. The velocity at t = 2 seconds drops to zero for r^* less than ~ 0.3 because this region is now devoid of liquid. Figure 17 shows a similar profile at $z^* = 0.1$. These two plots clearly show the marked effect of free surface deformation.

Figures 18 and 19 show the axial velocity profiles at two different vertical locations. The axial velocities are found to be higher for $z^* = 1$ compared to the forced region. At longer times, the free surface effects become more pronounced, and damp out the vertical velocities to a considerable extent.

5. Conclusions

In the paper we developed a formulation and presented computed results describing the behavior of a metal column subjected to a rotating magnetic field. In the formulation we provided a substantial extension of previous work by:

- allowing for the non - uniformity of the magnetic field, due to the end effects in the vicinity of the free metal surface
- allowing for the deformation of the free surface.

The principal findings of the work may be summarized as follows:

- In agreement with a recent publication by Davidson & Hunt (1987) we found that the "end effects" due to the finite coil size and the discontinuities at the free metal surface may give rise to significant secondary flows. More specifically, while the field is intended to produce a rotary motion, significant axial velocities will exist. The treatment presented here supports the findings of Davidson and Hunt, but enabled these calculations to be done with

a much greater degree of precision, both regarding the magnitude of the field and the melt velocities.

- In the calculations presented due allowance was made for free surface deformation. It was found that for the system considered, significant free surface deformation would occur; furthermore, if one were to impose artificially the existence of a flat free surface, not only would this introduce the obvious errors regarding the free surface shape, but would also significantly falsify the velocity fields in the vicinity of the free surface. The precise knowledge of free surface shapes and the velocities near the free surface is of major practical importance, because these quantities may play a very significant role in affecting the (surface) quality of continuous cast products — the main practical application of electromagnetic stirring.

6. Acknowledgements

This work was sponsored by the National Science Foundation under Research Grant # MSM-86-11879.

7. References

DAVIDSON, P. A. 1985 Estimation of Turbulent Velocities Induced by Magnetic Stirring during Continuous Casting. *Materials Science and Technology* **1**, 994-999.

DAVIDSON, P. A. 1988 Primary and Secondary Flows in the Rotary Magnetic Stirring of Molten Steel. In Branover H. & Mond M. (eds.) Proc. 5th. Beer-Sheva Seminar on MHD Flows and Turbulence, Prog. in Astro. and Aero., AIAA **111**, 442-463.

DAVIDSON, P. A. & BOYSAN, F. 1987 The Importance of Secondary Flow in the Rotary Electromagnetic Stirring of Steel During Continuous Casting. *Appl. Sci. Res.* **44**, 241-259.

DAVIDSON, P. A. & HUNT, J. C. R. 1987 Swirling recirculating flow in a liquid-metal column generated by a rotating magnetic field. *J. Fluid Mech.* **185**, 67-106.

FLORYAN, J. M. & RASMUSSEN, H. 1989 Numerical methods for viscous flows with moving boundaries. *Appl. Mech. Rev.* **42**, no. 12, 323-341.

HIRT, C. W. & NICHOLS, B. D. 1981 Volume of Fluid (VOF) method for the dynamics of free boundaries. *J. Comput. Phys.* **34**, 390-400.

ILEGBUSI, O. J. & SZEKELY, J. 1989 Three Dimensional Velocity Fields for Newtonian and Non-Newtonian Melts Produced by a Rotating Magnetic Field. *ISIJ International* **29**, no. 6, 462.

KITAGAWA, T., KAWAKAMI, K., MIZUKAMI, H. & NISHIOKA, S. 1983 Fundamental Study on the Application of Electromagnetic Stirring in Continuous Casting of Steel. *Proc. U.S.-Japan Coop. Sci. Program Seminar on "Solidification Processing", Dedham, MA, USA* 551-568.

LAUNDER, B. E. & SPALDING, D. B. 1972 *Mathematical Models of Turbulence.* Academic Press.

MOFFAT, H. K. 1965 On fluid flow produced by a rotating magnetic field. *J. Fluid Mech.* **22**, 521-528.

NICHOLS, B. D., HIRT, C. W. & HOTCHKISS, R. S. 1980 SOLA-VOF: A Solution Algorithm for Transient Fluid Flow with Multiple Free Boundaries. *Report LA-8355, Los Alamos Scientific Laboratory, Los Alamos, New Mexico, USA* 21.

POOLE, H. B.(publisher) 1986 Electromagnetic Stirring (EMS) During Continuous Casting of Steel–Literature Search and Installation Survey. *AISE.*

ROBINSON, T. 1973 An Experimental investigation of a magnetically driven rotating liquid-metal flow. *J. Fluid Mech.* **60**, 641-664. (With an Appendix by Larsson, K.)

SAHAJWALA, V., BRIMACOMBE, J. K. & SALCUDEAN, M. E. 1989 Spout formation at the free surface of gas stirred liquid. *SCANINJECT V, Part II, Proc. of the Fifth International Conference on Ladle Metallurgy, Lulea, Sweden* 103-144.

SALUJA, N. 1991 Electromagnetic Stirring of Metallic Melts — Theory and Experiments. Sc.D. Thesis, Department of Materials Science and Engineering, Massachusetts Institute of Technology, Cambridge, MA.

SALUJA, N., ILEGBUSI, O. J. & SZEKELY, J. 1990 On the Calculation of the Electromagnetic Force Field in the Circular Stirring of Metallic Melts. *J. App. Phys.*, **68** (11), 5845-5850.

SNEYD, A. 1971 Generation of fluid motion in a circular cylinder by an unsteady applied magnetic field. *J. Fluid Mech.* **49**, 817-827.

SPITZER, K. H., DUBKE, M. & SCHWERDTFEGER, K. 1986 Rotational Electromagnetic Stirring in Continuous Casting of Round Strands. *Metall. Trans. B* **7B**, 119.

TZAVARAS, A. A. & BRODY, H. D. 1984 Electromagnetic Stirring and Continuous Casting — Achievements, Problems, and Goals. *J. of Metals* 31.

8. Tables

TABLE 1. Turbulence constants used in the computations

C_v	C_k	C_{mk}	$C_{\varepsilon 1}$	$C_{\varepsilon 2}$	$C_{m\varepsilon}$
0.09	1.0	1.0	1.44	1.92	0.77

TABLE 2. Input parameters for the computations

Melt	Steel
Density (kg m^{-3})	7022.0
Kinematic Viscosity (m^2 s^{-1})	7.8325×10^{-7}
Amplitude of Applied Magnetic Field (tesla)	0.05
Electrical Conductivity of Steel Melt (A V^{-1} m^{-1})	7.14×10^5
Angular Velocity of the Field (rpm)	1200.0
Surface Tension Coefficient (N m^{-1})	1.872
Contact Angle (Degrees)	135
Electrical Conductivity of Copper Mould (A V^{-1} m^{-1})	5.7×10^7

Table 3. Geometry used in the computations

Case	r_o (m)	h_m (m)	h_s (m)	h_l (m)
1	0.06	0.45	0.25	0.1
2	0.20	1.0	0.20	0.4

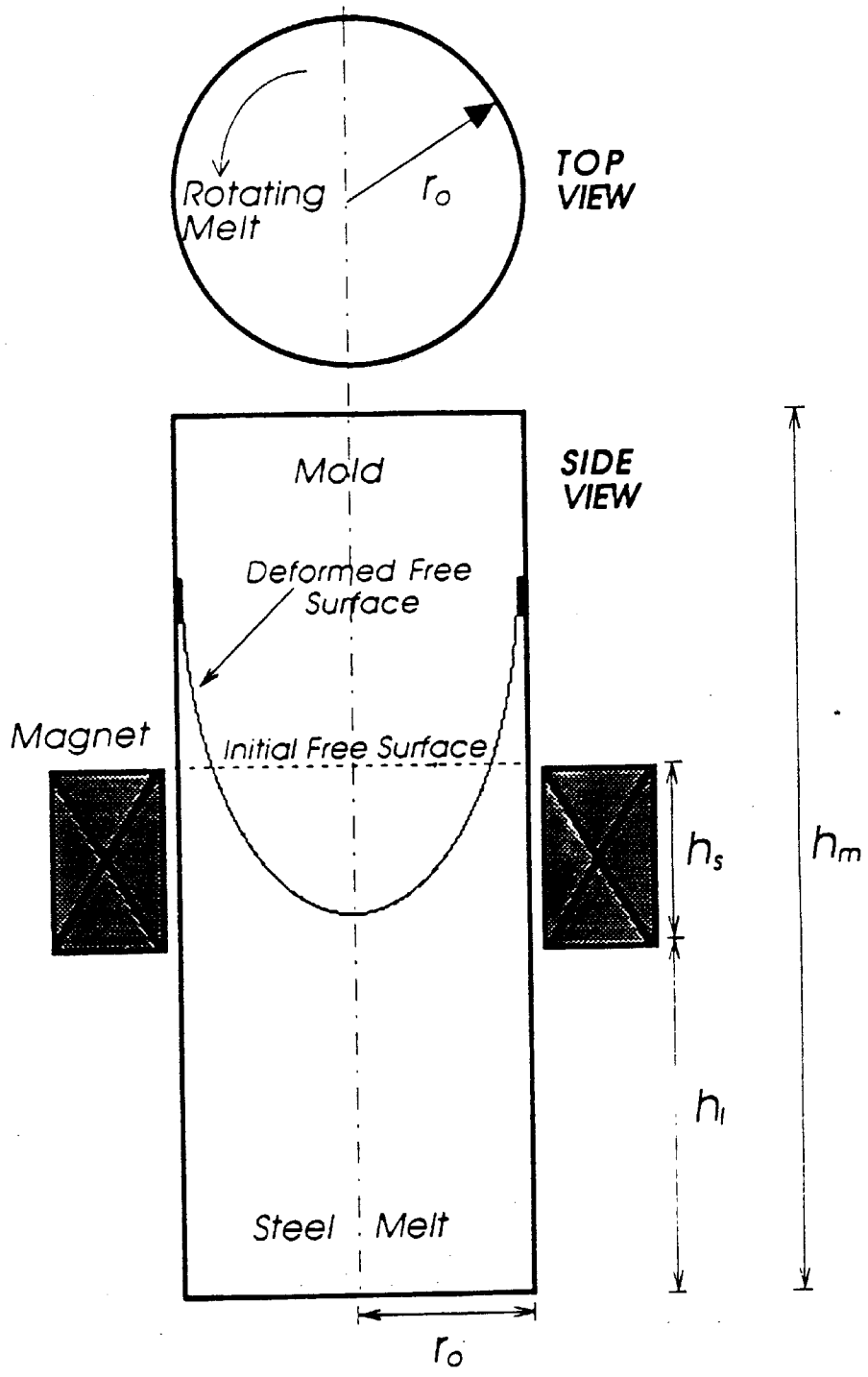

Figure 1. Schematic diagram of a typical electromagnetically stirred system.

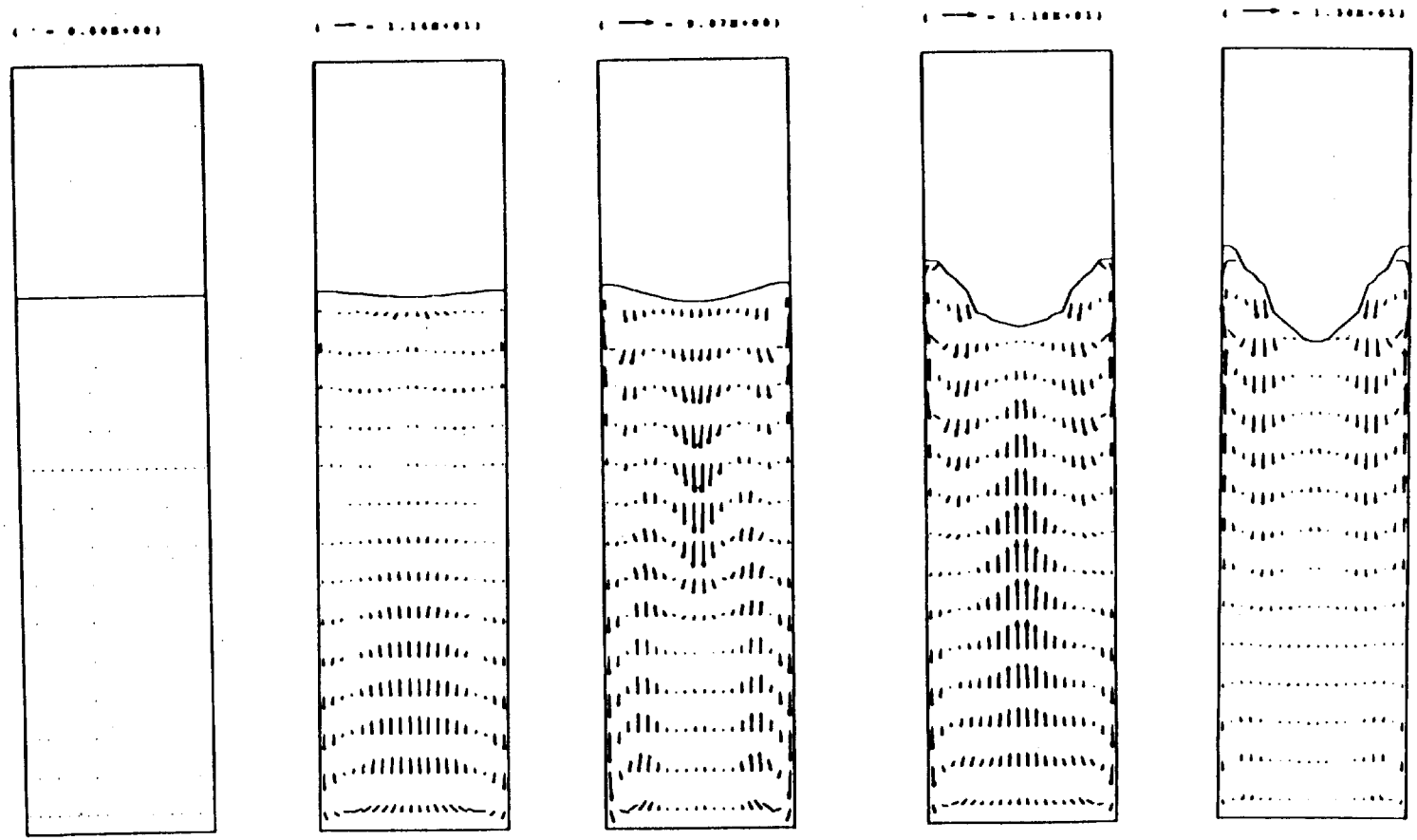

(a) t = 0 s (b) t = 1 s (c) t = 2 s (d) t = 3 s (e) t = 4 s

Figure 2. Velocity fields for the system at various times (a) $t = 0$ seconds; $v_{max} = 0.0$ cm/s (b) $t = 1$ seconds; $v_{max} = 11.4$ cm/s (c) $t = 2$ seconds; $v_{max} = 9.87$ cm/s (d) $t = 3$ seconds; $v_{max} = 11.8$ cm/s, and (e) $t = 4$ seconds.; $v_{max} = 13.0$ cm/s.

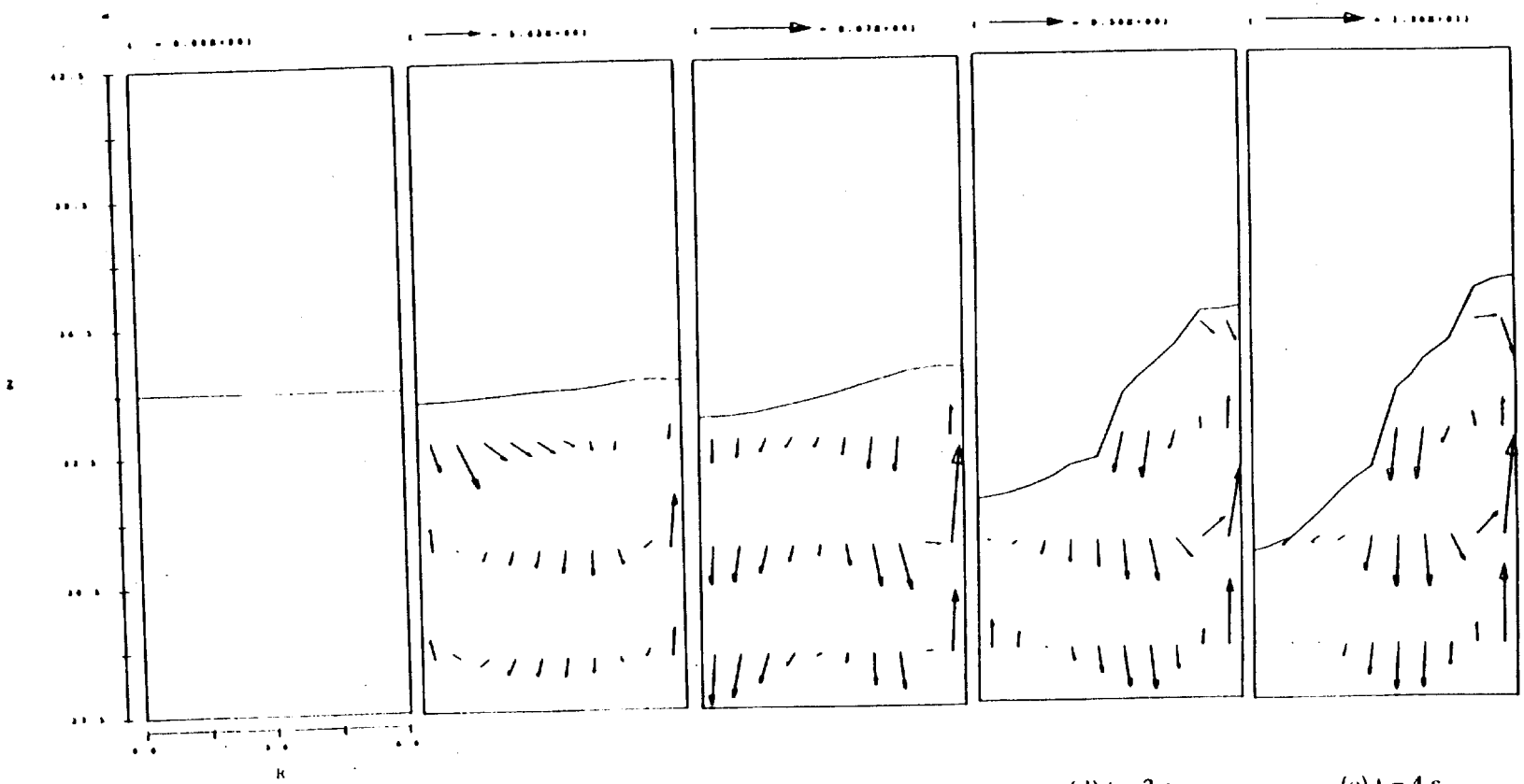

(a) t = 0 s (b) t = 1 s (c) t = 2 s (d) t = 3 s (e) t = 4 s

Figure 3. Velocity vectors in the vicinity of the top surface (free surface)
(a) $t = 0$ seconds $v_{max} = 0.0$ cm/s
(b) $t = 1$ seconds $v_{max} = 5.62$ cm/s
(c) $t = 2$ seconds $v_{max} = 9.87$ cm/s
(d) $t = 3$ seconds $v_{max} = 9.50$ cm/s
(e) $t = 4$ seconds. $v_{max} = 13.0$ cm/s.

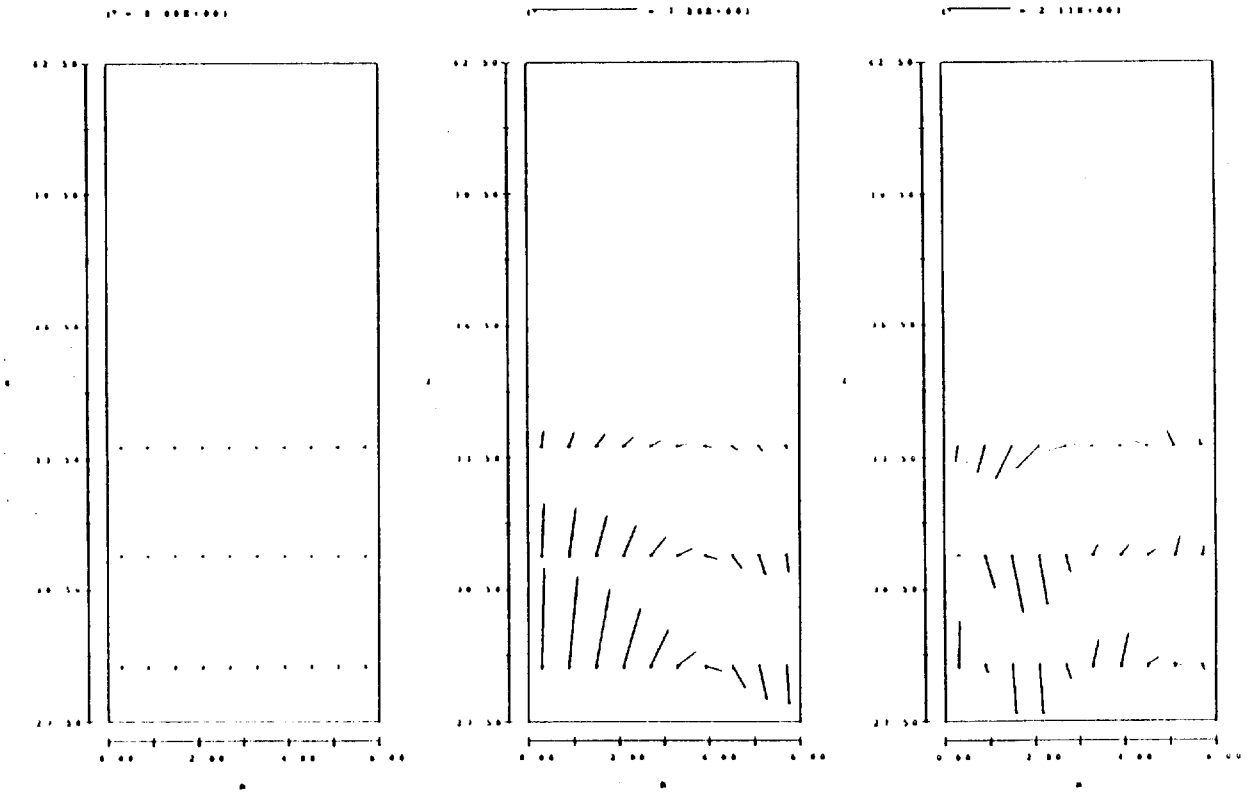

(a) t = 0 s (b) t = 1 s (c) t = 2 s

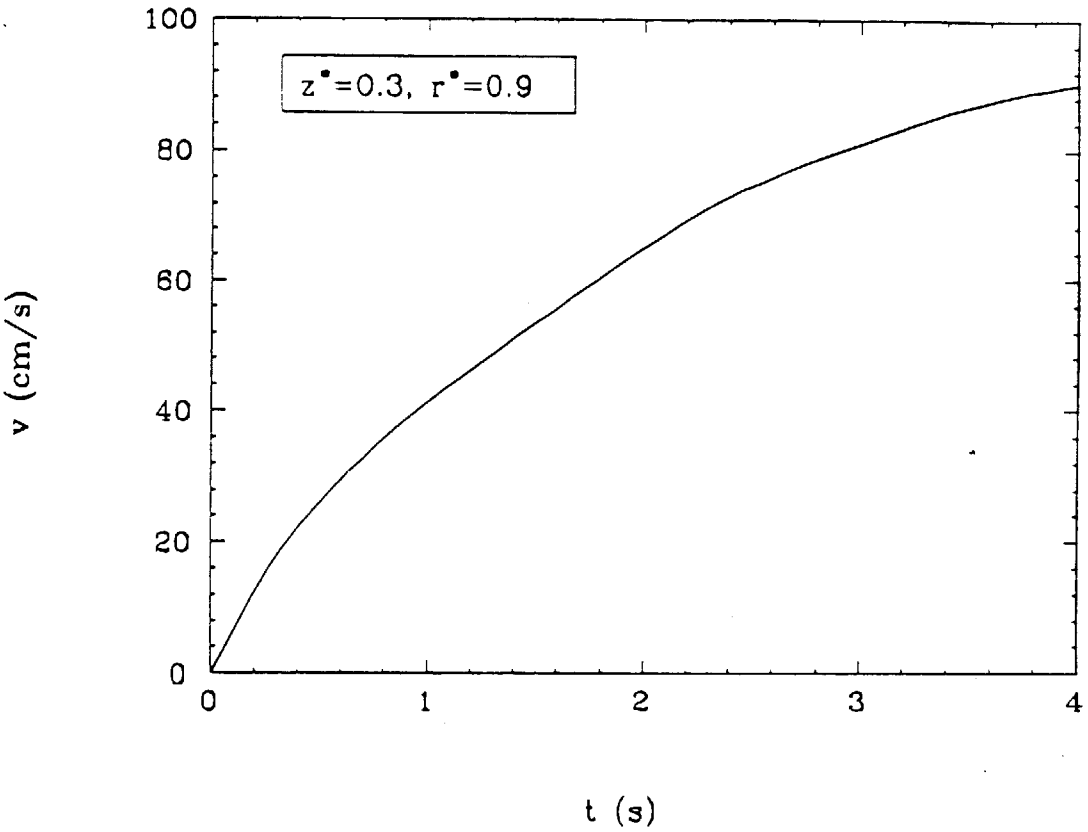

Figure 5. Plot for the history of the azimuthal velocity at monitored location at $z^* = 0.3$ and $r^* = 0.9$.

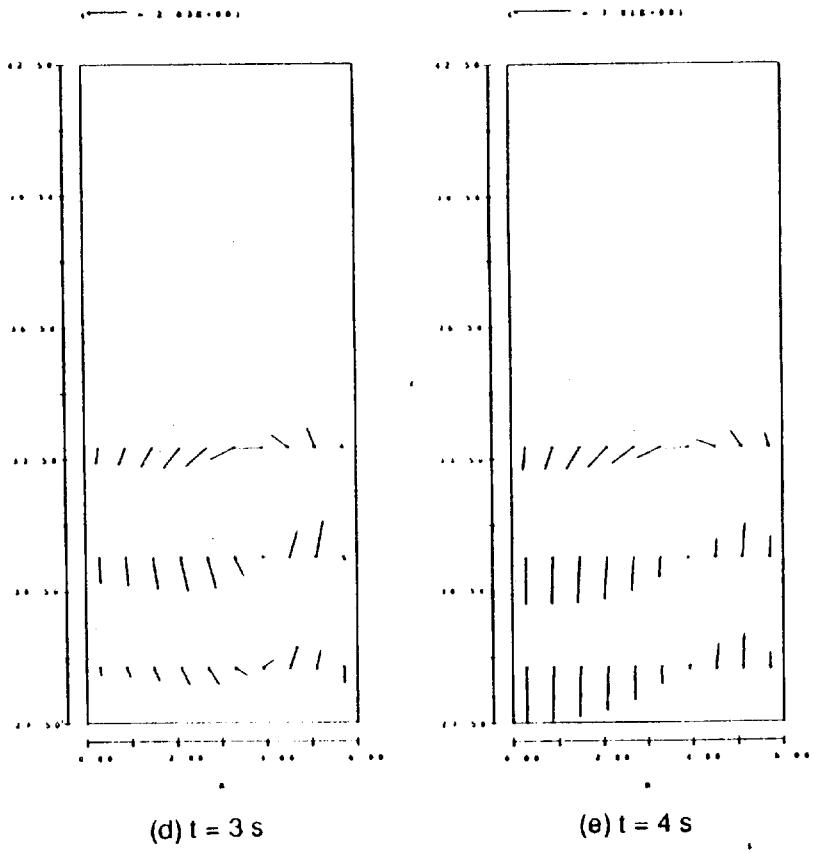

Figure 4.

Velocity vectors in the vicinity of a rigid top surface

(a) $t = 0$ seconds $v_{max} = 0.0$ cm/s
(b) $t = 1$ seconds $v_{max} = 7.28$ cm/s
(c) $t = 2$ seconds $v_{max} = 2.11$ cm/s
(d) $t = 3$ seconds $v_{max} = 2.83$ cm/s
(e) $t = 4$ seconds. $v_{max} = 7.01$ cm/s.

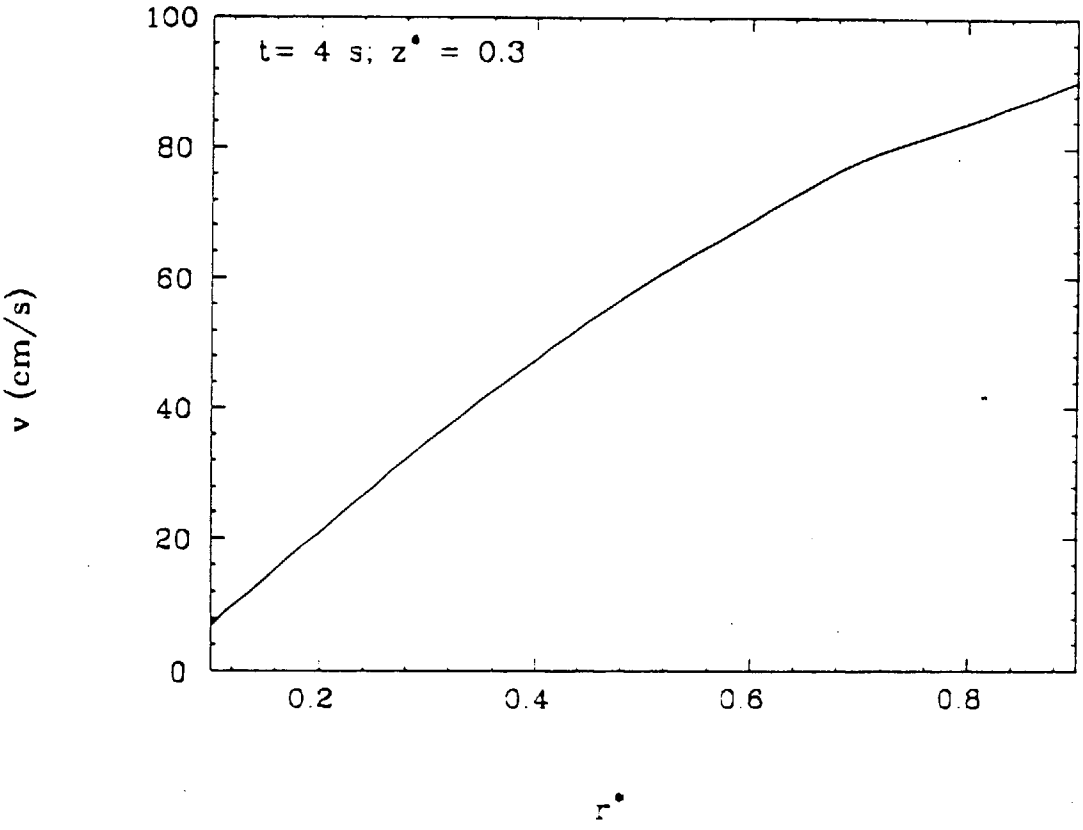

Figure 6. Profile of the azimuthal velocity in the radial direction at a height of 15 cm ($z^* = 0.3$) at $t = 4$ seconds.

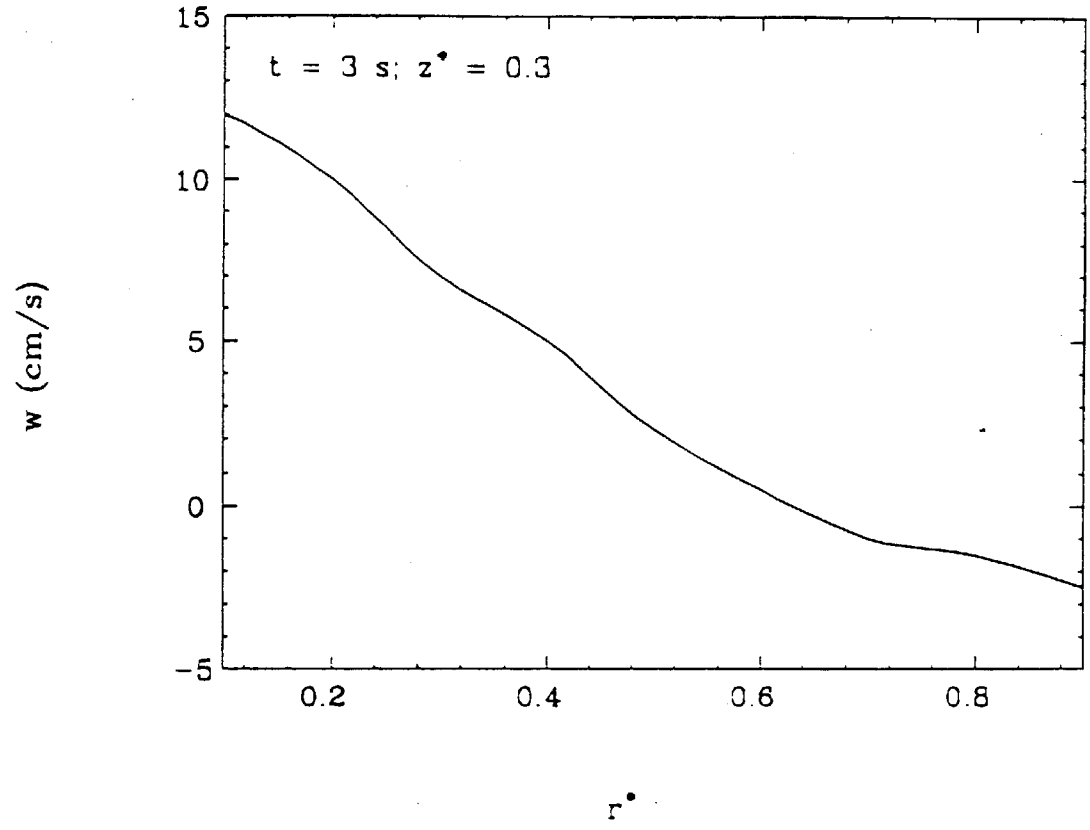

Figure 7. Profile of the axial velocity in the radial direction at a height of 15 cm ($z^* = 0.3$) at $t = 3$ seconds.

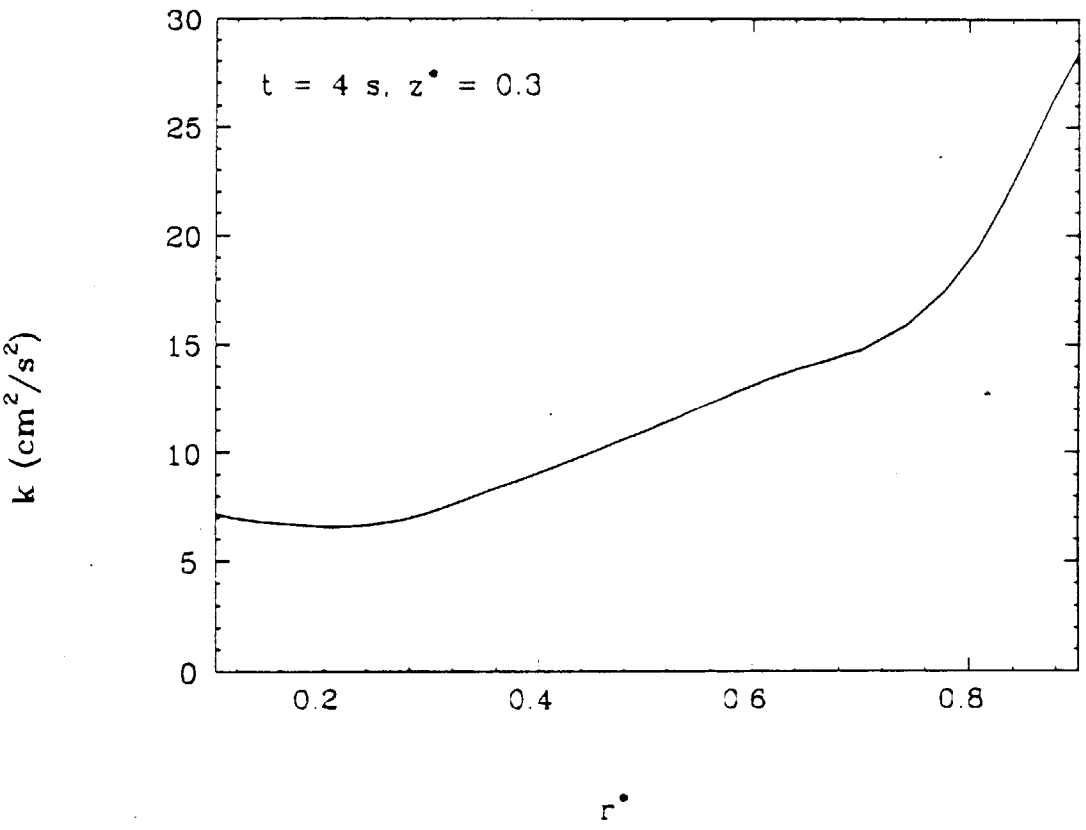

Figure 8. Profile of the turbulence kinetic energy in the radial direction at a height of 15 cm ($z^* = 0.3$) and at $t = 4$ seconds.

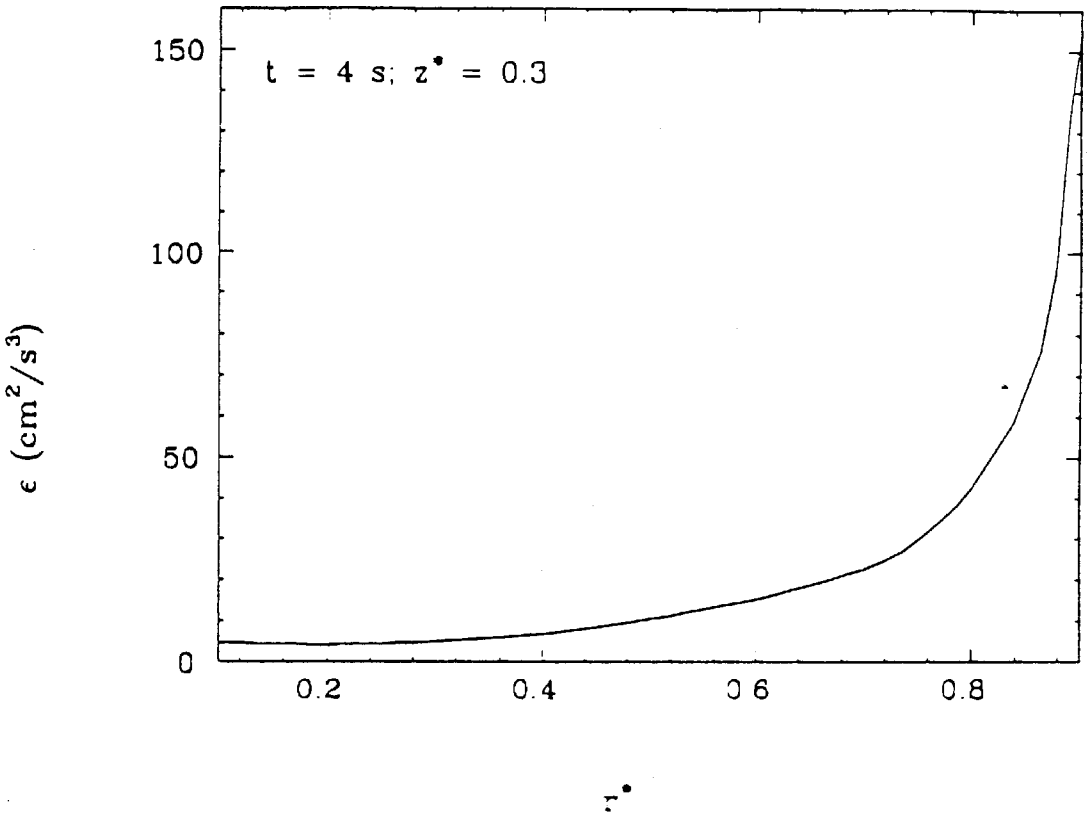

Figure 9. Profile of the turbulence energy dissipation in the radial direction at a height of 15 cm ($z^* = 0.3$) and at $t = 4$ seconds.

Figure 10.
Velocity fields at t = 0.5 seconds. The upper and lower magnifications show the velocity fields in the vicinity of the free surface and below the stirrer respectively. v_{max} = 24.8 cm/s.

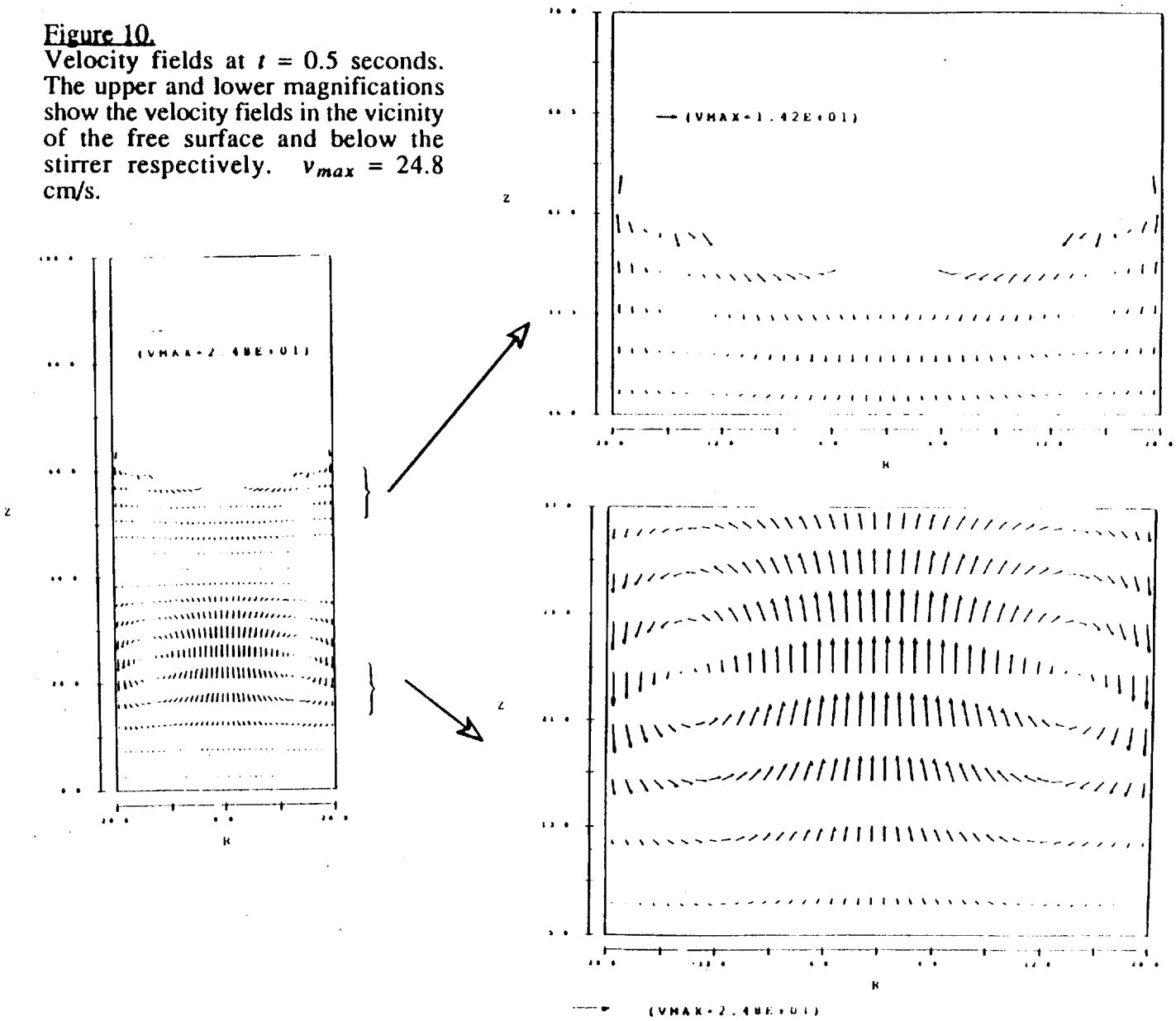

Figure 11.
Velocity fields at t = 1.0 seconds. The upper and lower magnifications show the velocity fields in the vicinity of the free surface and below the stirrer respectively. v_{max} = 76.8 cm/s.

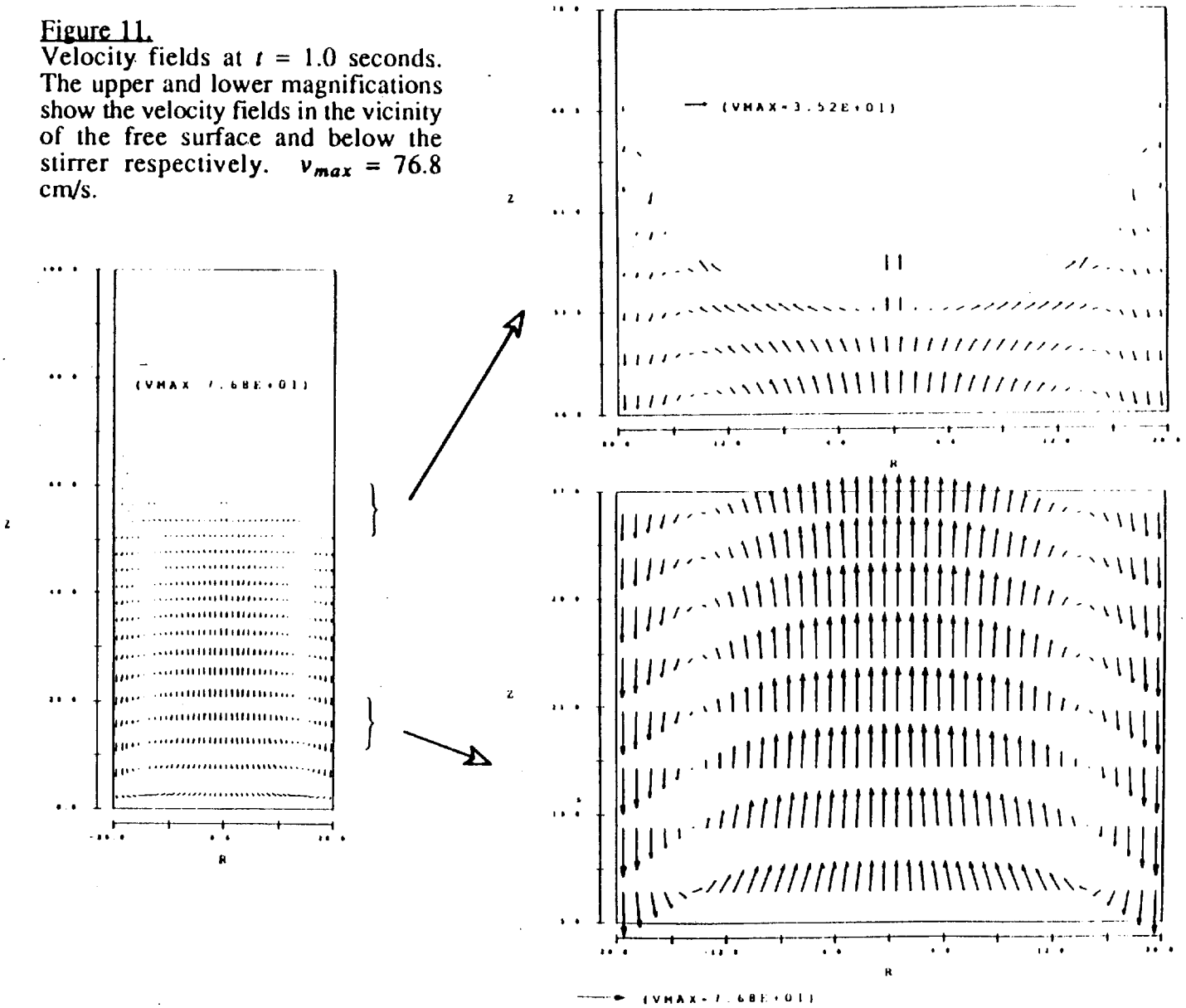

Figure 12.
Velocity fields at t = 2.0 seconds. The upper and lower magnifications show the velocity fields in the vicinity of the free surface and below the stirrer respectively. v_{max} = 78.9 cm/s.

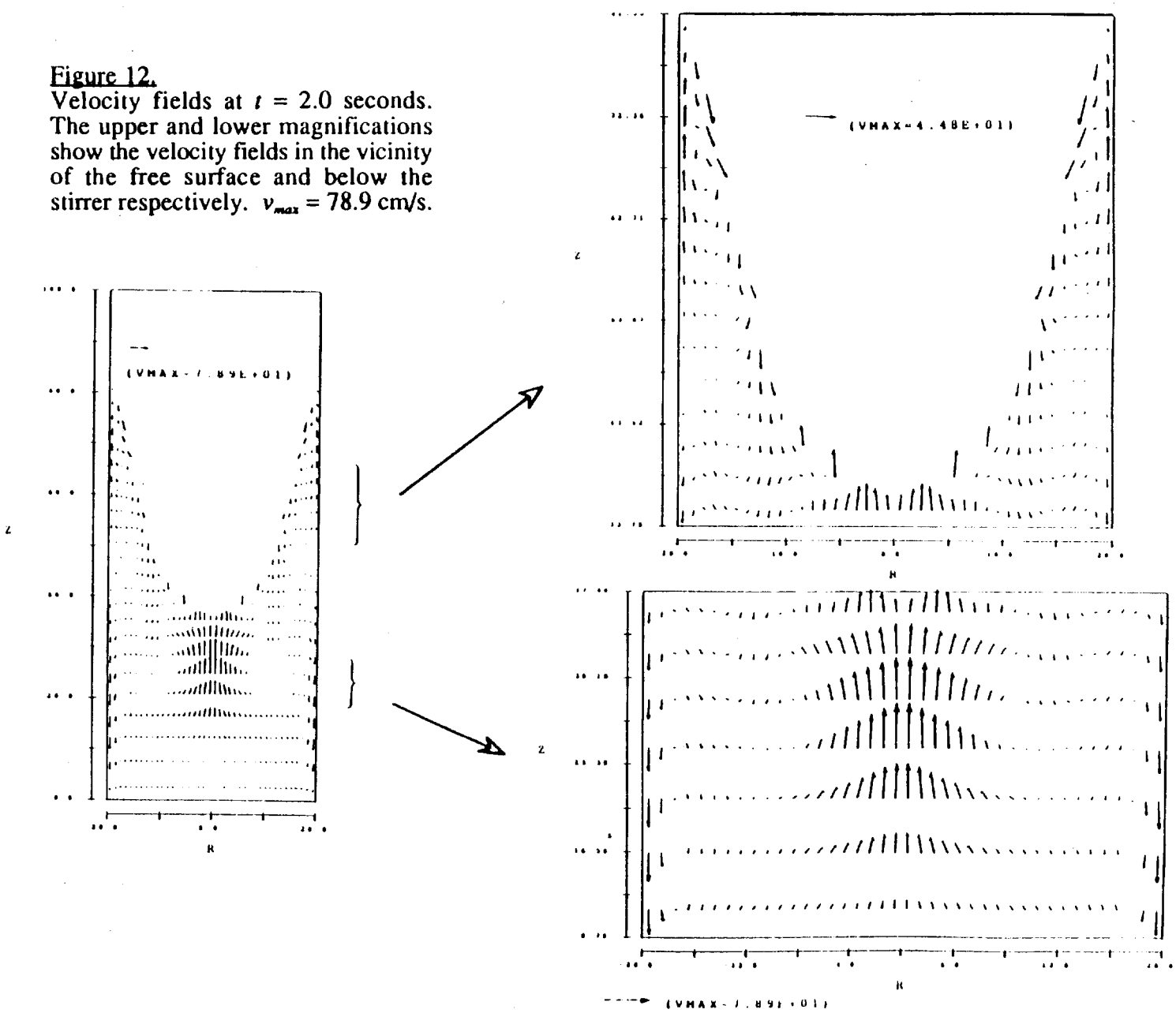

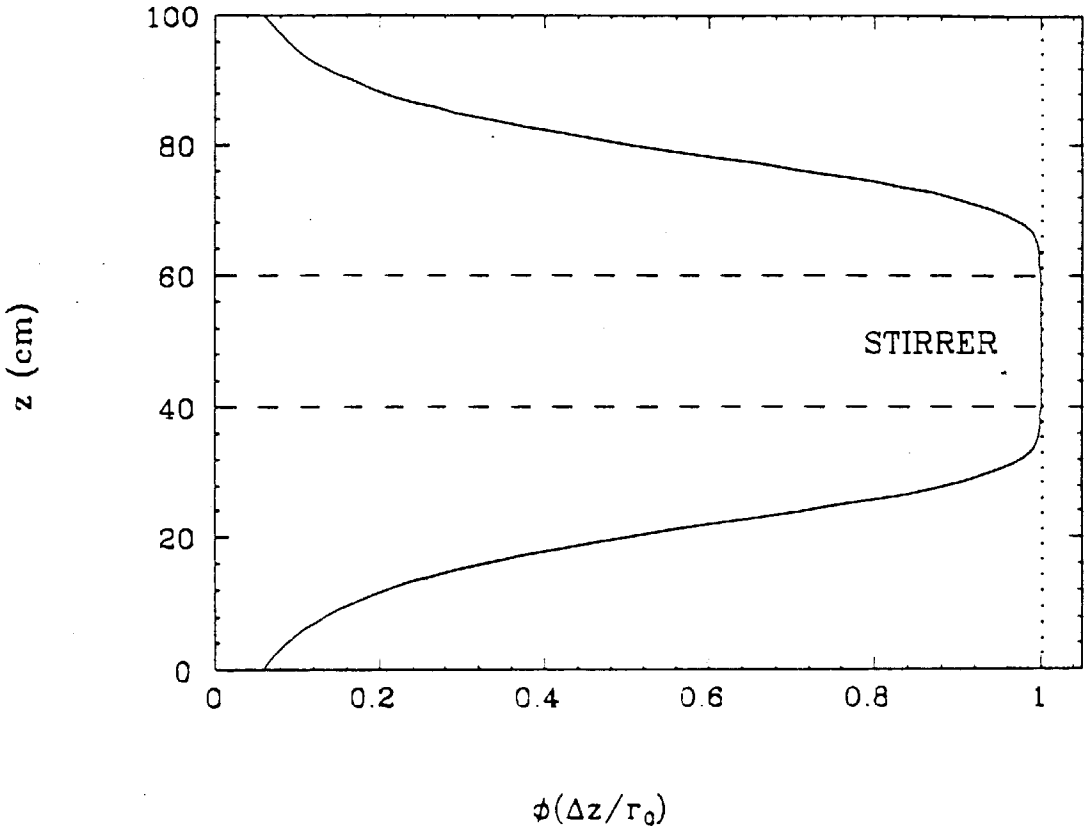

Figure 13. The axial variation of electromagnetic forces, showing a fourth power-law decay.

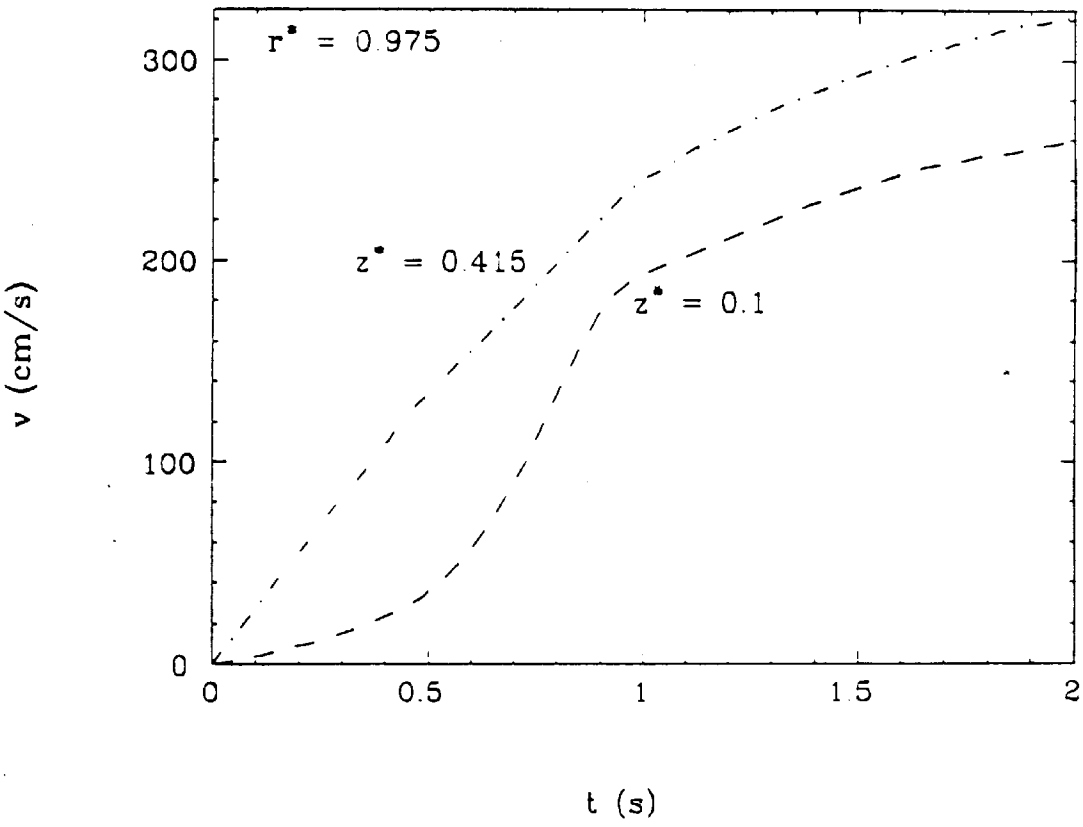

Figure 14. The evolution of azimuthal velocity at $r^* = 0.975$ at two different heights.

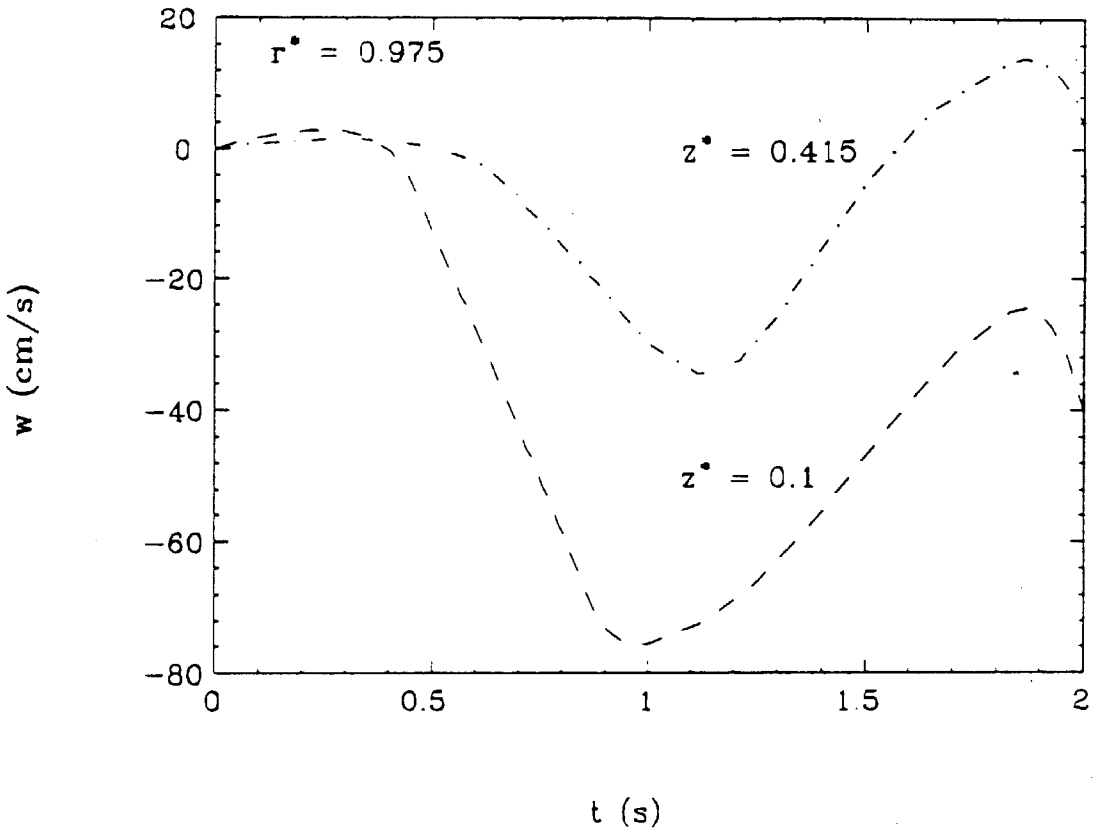

Figure 15. The evolution of axial velocity at $r^* = 0.975$ at two different heights.

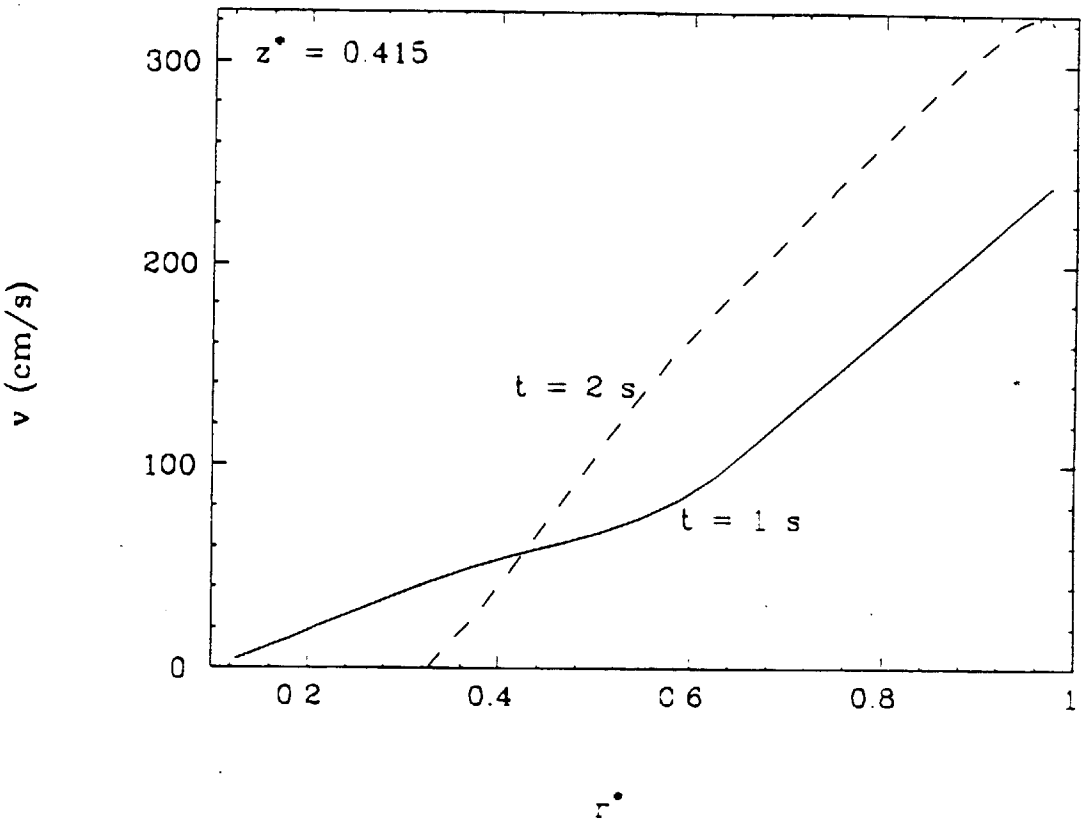

Figure 16. Radial profile of the azimuthal velocity at $z^* = 0.415$ at times of 1.0 and 2.0 seconds.

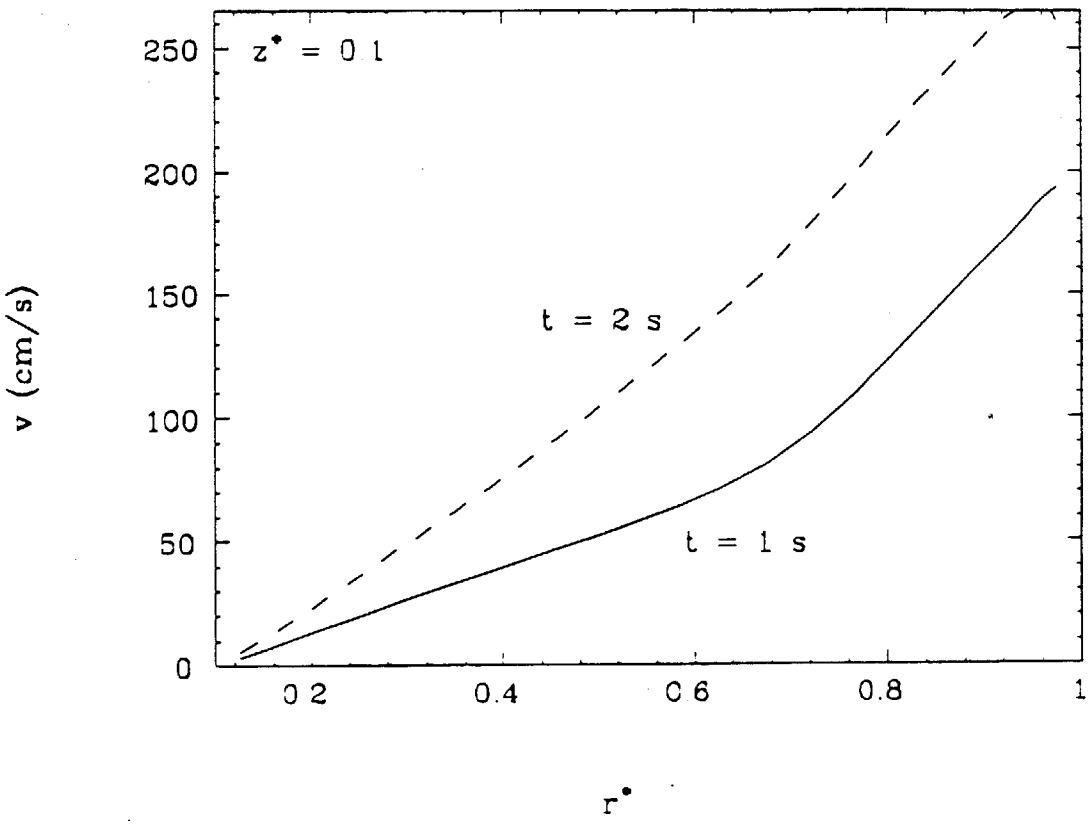

Figure 17. Radial profile of the azimuthal velocity at $z^* = 0.1$ at times of 1.0 and 2.0 seconds.

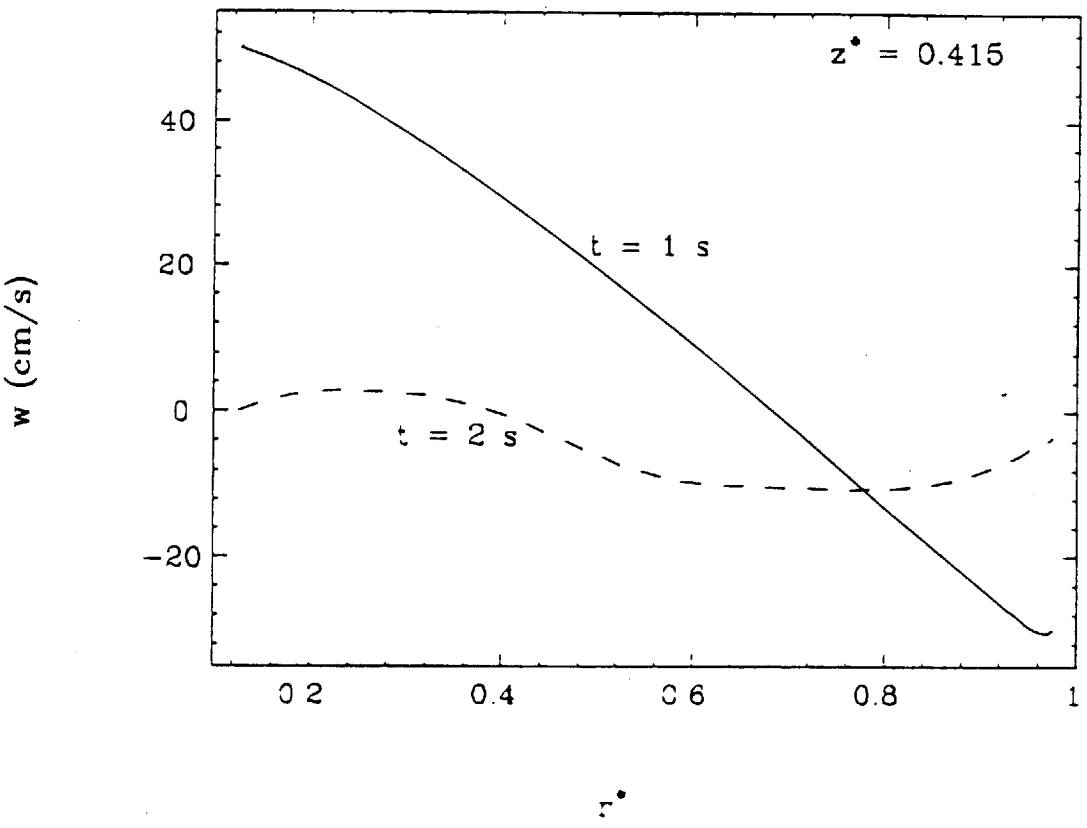

Figure 18. Radial profile of the axial velocity at $z^* = 0.415$ at times of 1.0 and 2.0 seconds.

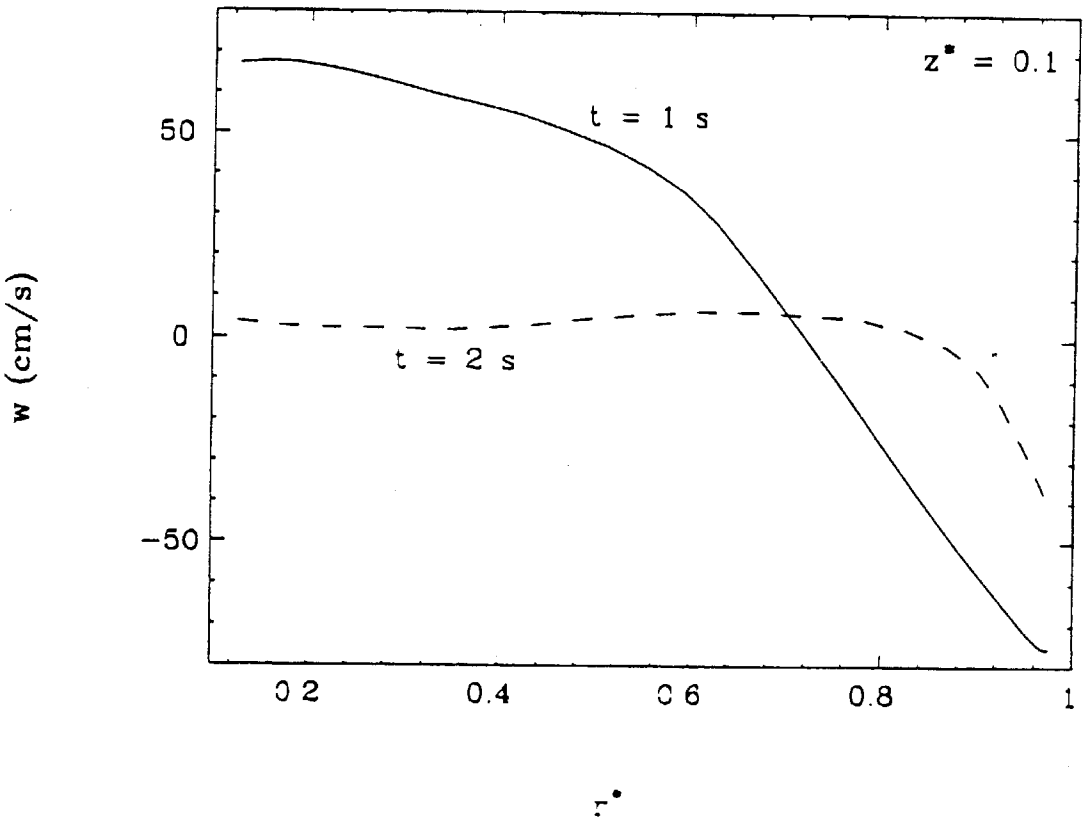

Figure 19. Radial profile of the axial velocity at $z^* = 0.1$ at times of 1.0 and 2.0 seconds.